

The structure of warm dense matter modeled with an average atom model with ion-ion correlations

D. Saumon, C.E. Starrett, J.A. Anta, W. Daughton and G. Chabrier

Abstract We present a new model of warm dense matter that represents an intermediate approach between the relative simplicity of “one-ion” average atom models and the more realistic but computationally expensive *ab initio* simulation methods. Physical realism is achieved primarily by including the correlations in the plasma that surrounds a central ion. The plasma is described with the Ornstein-Zernike integral equations theory of fluids, which is coupled to an average atom model for the central ion. In this contribution we emphasize the key elements and approximations and how they relate to and expand upon a typical average atom model. Besides being relatively inexpensive computationally, this approach offers several advantages over *ab initio* simulations but also has a number of limitations. The model is validated by comparisons with numerical solutions for the pair distribution function of the ions from *ab initio* simulations for several elements and a wide range of plasma conditions. Simulations results are reproduced remarkably well and simpler limiting theories are recovered as well. This model has many potential applications to calculation of the properties of warm dense matter such as the equation of state and conductivities for a wide range of temperatures and densities.

D. Saumon, C.E. Starrett and W. Daughton
Los Alamos National Laboratory, P.O. Box 1663, Los Alamos, NM 87545, USA e-mail:
dsaumon@lanl.gov, starrett@lanl.gov, daughton@lanl.gov

J.A. Anta
Dept. Sistemas Físicos, Químicos y Naturales, Universidad Pablo de Olavide, Ctra. Utrera, km 1 -
41013 Sevilla, Spain e-mail: anta@upo.es

G. Chabrier
CRAL (UMR CNRS 5574), École Normale Supérieure de Lyon, 69364 Lyon Cedex 07, France
e-mail: chabrier@ens-lyon.fr

1 Introduction

Warm dense matter (WDM) is an “inner” frontier of research in material properties in the sense that it is circumscribed by regimes that can be described by well-understood theoretical approaches and well-known limits. For instance, neither condensed matter theory, which is primarily based on treating electrons at near-zero temperature in periodic structures, nor plasma physics theory, based on small Coulomb coupling between the constitutive particles, are applicable to modeling WDM. More specifically, WDM is a partially ionized, globally neutral plasma characterized by moderate to strong coupling between all charged particles (ion-ion, ion-electron, and electron-electron) and partial electron degeneracy, where weakly bound states can cross into the continuum (pressure ionization). Depending on the material, this corresponds to temperatures of $\sim 1 - 100\text{eV}$ and densities of $\sim 0.1 - 50$ times the normal solid density. A general but admittedly vague definition of WDM, is that it occurs in the physical regime where “all the physics” is important. By definition, it is thus quite challenging to model.

Experimentally, WDM states are not particularly difficult to achieve nowadays as many experiments cross the WDM regime on their way to denser and, more often, hotter final states. The difficulty is in making a sample of WDM that is large enough, that is relatively long-lived and with a spatial homogeneity that allow meaningful probing of its properties. The nature of WDM also limits the effectiveness of well-established diagnostics of dense matter and plasmas and new methods need to be developed [1]. There is presently only a limited but growing amount of data on WDM states [2, 3, 4, 5, 6, 7, 8, 9, 10].

Despite the experimental and theoretical challenges it presents, WDM has long been of interest as it occurs naturally in the giant planets of the solar system (Jupiter, Saturn, Uranus and Neptune) [11, 12], in dense stars such as in the envelopes of white dwarf stars (the final stage of a star’s life) [13] and in the many giant and exotic planets that have been discovered orbiting other stars in the last decade [14]. In the laboratory, WDM is a transient state of imploding capsules in inertial confinement fusion experiments and can be produced with pulsed-power platforms and high-power laser facilities. Modeling these physical systems typically requires a knowledge of the equation of state, opacity, conductivity, and diffusion coefficients of WDM.

The intrinsic interest of WDM as a hard physics problem, as well as its importance to other fields of research has led to many approximate models that have steadily increased in sophistication. One large and important class of models, known as average atoms (AA) models, has a long history and have proved to be very useful. An AA model is essentially a one-ion model that solves for the electronic structure (bound and free states) around a central nucleus embedded in a spherically averaged, homogeneous plasma outside the ion sphere. There are many variants of such models but they all assume spherical symmetry and that the resulting modeled ion, which typically has a fractional net charge, represents in some sense an average of the multiple ion configurations (ionic states) present in the plasma. The assumptions about the surrounding plasma effectively replace the environment of the central ion

by a boundary condition at the radius of the ion sphere R defined by

$$\frac{4\pi R^3}{3} = \frac{1}{n_I^0} \quad (1)$$

where n_I^0 is the number density of ions. The system of equations defining an AA model (see §2 below) amounts to a self-consistent field problem in spherical symmetry and finite temperature. This is a conceptually straightforward problem which explains their early and long-lasting popularity to model WDM.¹ Through the boundary condition applied at the ion sphere radius, AA models can qualitatively, and to a fair extent, quantitatively, predict the electronic structure and charge of ions as a function of density and temperature [17, 18]. Despite their popularity and usefulness, average atom models account for the surrounding plasma only in the simplest possible way and ignore the correlations in the plasma, an important characteristic of WDM.

At the other end of the spectrum of complexity are computer simulations of WDM, based on *ab initio* methods such as Path Integral Monte Carlo (PIMC) and Quantum Molecular Dynamics (QMD) [19, 20, 21, 22, 23, 24, 25]. These methods take a more direct approach to solving the quantum many-body problem of WDM and use few approximations in simulating the properties of a mixture of nuclei and electrons in a simulation box. Bound and free states, radial and angular correlations, the formation of clusters, and multiple ion configurations naturally occur in such simulations. The theoretical appeal of these methods is tempered by their considerable computational cost even in view of the computing power available today. Simulations of higher- Z elements remain very onerous.

We present a new model of WDM that takes an intermediate path between simple average atom models and expensive simulations, with the goal of producing realistic material properties at a reasonable computational cost. The concept of the average atom is extended by including correlations between charged particles in the surrounding plasma. The structure of the central ion is thus solved in the field of the central nucleus and of the surrounding, correlated ions and electrons. This reintroduces the surrounding plasma correlations in a much more realistic fashion. By maintaining spherical symmetry in the formulation of the model, the computational cost remains modest. This opens the possibility of generating large tables of properties, particularly of the equation of state, that can be used in various applications. Similar models have been published in the past [26, 27, 28, 29] but this new model is based on a more formal derivation and a higher level of internal consistency. Limitations of earlier models have been overcome, resulting in a model that is applicable to a broad range of physical regimes, from liquid metals to WDM and high-temperature plasmas.

We first briefly review a typical average atom model in §2 to set the context for its extension to include plasma correlations. The full model is described in §3, with illustrations of the key models quantities. The models has been applied to a wide

¹ Achieving accurate numerical solutions is more challenging [15] but has progressed considerably [16].

range of elements, temperature and densities, and it has been validated by comparisons with *ab initio* simulations, primarily in terms of pair distribution functions (§4). The last section (§5) offers a summary and outlook. This contribution emphasizes the concepts that underlie the model and how it differs from previous similar efforts. A detailed presentation along with derivations are given in [30], where additional numerical results can also be found.

2 Average atom models

An average atom model describes a single central nucleus of charge Z with Z electrons embedded in a radially and spherically smoothed plasma residing outside the ion sphere surrounding the nucleus. The surrounding plasma has number density n_I^0 and, like the central ion, is at a temperature $T = 1/\beta$. Average atom models invariably describe the electron cloud surrounding the nucleus with the finite temperature formulation of the Kohn-Sham density functional theory (DFT) [31, 32, 33]. The latter can be cast in the semi-classical Thomas-Fermi model of the electrons [34, 35, 36], a full quantum mechanical description with the Schrödinger equation [37], or the relativistic quantum mechanical Dirac equation [38, 16, 18]. For the clarity of the discussion and without loss of generality, hereafter we will consider only the quantum mechanical case (Schrödinger equation). The structure of a typical AA model and its key equations are shown in Fig. 1, which is a guide to the following discussion of the model. The effective one-electron DFT Schrödinger equation is

$$[\hat{T} + V_{Ne}^{\text{eff}}(r)]\psi_i(r) = \varepsilon_i\psi_i(r) \quad (2)$$

where \hat{T} is the kinetic energy operator, $V_{Ne}^{\text{eff}}(r)$ is the effective one-electron potential energy, $\psi_i(r)$ is the one-electron radial wave function of state i with energy ε_i . The outer boundary condition is applied at $r \rightarrow \infty$ where $V_{Ne}^{\text{eff}} \rightarrow 0$ and a free particle solution is obtained. $\psi_i(r) \rightarrow 0$ at infinity for bound states. For continuum states, $\psi_i(r \rightarrow \infty)$ is required to match the free solution (spherical Bessel function). In practice, the outer boundary condition is applied at some large radius R_{max} that defines the edge of the computational boundary, where $\psi_i(R_{\text{max}})=0$ for bound states, and $\psi_i(R_{\text{max}})$ is matched to spherical Bessel functions for continuum states [39]. The potential is

$$V_{Ne}^{\text{eff}}(r) = -\frac{Z}{r} + \int \frac{n_e(r') - Z^*n_I(r')}{|\mathbf{r} - \mathbf{r}'|} d^3r' + V_{xc}^{ee}[n_e(r)] - V_{xc}^{ee}[n_e^0] \quad (3)$$

where $n_e(r)$ and $n_I(r)$ are the radial density profiles of electrons and ions around the central nucleus, respectively, Z^* is the ion charge in the average atom model, and V_{xc}^{ee} is the electron exchange and correlation potential. The electron density is obtained by summing the density associated with the eigenfunctions of both bound and continuum states

$$n_e(r) = 2 \sum_{i=\text{bound}} g_i |\psi_i(r)|^2 + \frac{2}{(2\pi)^3} \int_{\text{cont}} d^3k g_k |\psi_k(r)|^2 \quad (4)$$

and the free electron density is

$$n_e^0 = \lim_{r \rightarrow \infty} n_e(r). \quad (5)$$

The g_i and g_k are Fermi occupation factors

$$g_i = \frac{1}{e^{\beta(\epsilon_i - \mu_e^{\text{id}})} + 1}, \quad (6)$$

where μ_e^{id} is the ideal chemical potential of the electrons. Global neutrality of the plasma requires that the ion charge be

$$Z^* = n_e^0 / n_I^0. \quad (7)$$

This essentially defines the self-consistent field problem of the AA model.

Two additional elements are needed to close this system of equations, neither of which is unique (green boxes in Fig. 1). One is the density profile of the ions surrounding the central nucleus, $n_I(r)$, which describes the surrounding plasma. In AA models, this is taken as a simple step function with a constant ion density outside the ion sphere:

$$n_I(r) = n_I^0 \Theta(r - R), \quad (8)$$

which describes a cavity (the ion sphere) in the plasma centered at the origin. This form was originally devised to approximate the periodic nature of solids in AA models [40, 26], by confining each average atom within the ion sphere² but it can also be interpreted as the ion pair distribution function in a dense plasma. With this choice for $n_I(r)$, the average atom is coupled to the external plasma only through the ion sphere radius R , which depends only on the density n_I^0 . This choice of $n_I(r)$ implies that the external ions are not correlated with each other or with the central nucleus. It has the virtue of extreme simplicity but is clearly quite approximate and leaves out important physics.

The second element is the chemical potential μ_e^{id} of non-interacting electrons which determines the Fermi occupation factors g_i and g_k in the electron density (Eq. 6). This can be determined in several different ways. A very common practice [38, 16, 18, 26] is to use a local charge neutrality condition. For example

$$Z = \int_0^R n_e(\mu_e^{\text{id}}, r) d^3r, \quad (9)$$

where the μ_e^{id} dependence of $n_e(r)$ is shown explicitly, ensures neutrality within the volume of the ion sphere. This relation uniquely determines μ_e^{id} . The free electron density that corresponds to $V_{N_e}^{\text{eff}}(r \rightarrow \infty) = 0$ then follows from

² In this case the boundary condition is applied at $r = R$.

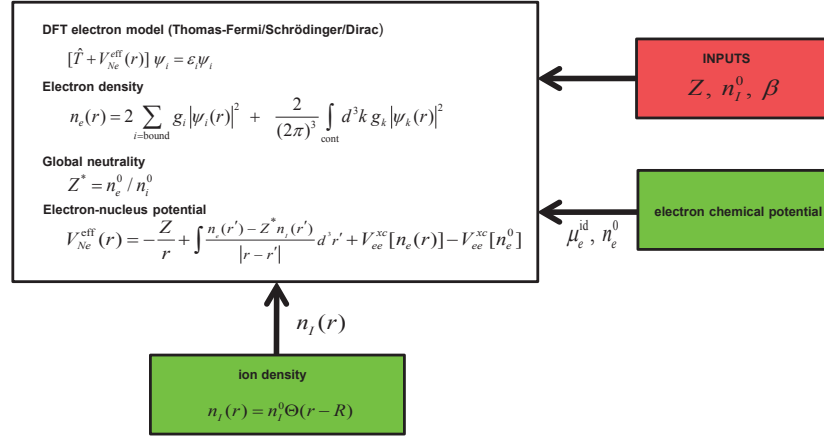


Fig. 1 Structure and key equations of a typical average atom model. The red box gives the input parameters to the model. Green boxes show model components where other choices are possible. Arrows show the flow of information between the key elements of the model. See text for details.

$$n_e^0 = \frac{\sqrt{2}}{\pi^2 \beta^{3/2}} \int \frac{x^{1/2} dx}{e^{x - \beta \mu_e^{id}} + 1}, \quad (10)$$

which also determines the ion charge Z^* (Eq. 7). It is well known that there is no rigorous definition of the ion charge in AA models [18, 17]. While Eq. (9) is intuitively sensible, there are other intuitively reasonable choices [17, 27, 28, 41, 42], such as requiring that $Z = N_b + n_e^0/n_i^0$, where N_b is the number of electrons bound to the central nucleus

$$N_b = 2 \int \sum_{i=\text{bound}} g_i |\psi_i(r)|^2 d^3r \quad (11)$$

(see Eq. 4). This is equivalent to requiring that the ion charge is that of the nucleus minus the number of bound electrons: $Z^* = Z - N_b$. It has been shown [18] that requiring that the AA model gives the same pressure whether obtained from the virial or thermodynamic routes gives a condition for μ_e^{id} that involves the electrostatic potential rather than the electron density:

$$\int_0^\infty d^3r \Theta(r-R) V_{Ne}^{el}(r) = 0, \quad (12)$$

where

$$V_{Ne}^{el} = -\frac{Z}{r} + \int \frac{n_e(r') - Z^* \Theta(r'-R)}{|\mathbf{r} - \mathbf{r}'|} d^3r'. \quad (13)$$

This result is obtained by minimizing the AA free energy with respect to n_e^0 . Paradoxically, this more rigorous approach to determine μ_e^{id} gives anomalously low values of Z^* at low temperatures [18], where it fares worse than models using a local neutrality condition such as Eq. (9). It appears that this more rigorous AA model exposes a detrimental aspect of neglecting the correlations in the surrounding plasma, a feature that must be partly compensated in models that use an ad hoc local neutrality condition.

To summarize, the AA model is a DFT-based, spherically symmetric, self-consistent field atom model embedded in a plasma. The equations are closed with two additional inputs: 1) an external ion distribution function which defines a cavity in a homogeneous (uncorrelated) plasma, and 2) a criterion to determine the non-interacting (field-free) part of the chemical potential of the electrons. The latter cannot be uniquely defined and various sensible choices give different results for the electronic structure of the central ion. The former is a simple and convenient approximation that can be improved upon. In fact, the absence of plasma correlations in the AA model is the most significant piece of physics that is missing in AA models. We now expand the AA model to include interactions within the surrounding plasma and with the central ion while preserving the assumption of spherical symmetry.

3 An average atom model with plasma correlations

The importance of the correlations in the surrounding plasma was recognized decades ago and several models have been developed to account for them [43, 27, 28, 26]. They affect the AA model shown in Fig. 1 in two ways. First the effective nucleus-electron potential now includes interactions between the electrons and the surrounding ions:

$$V_{Ne}^{\text{eff}}(r) = -\frac{Z}{r} + \int \frac{n_e(r') - Z^*n_I(r')}{|\mathbf{r} - \mathbf{r}'|} d^3r' + V_{xc}^{ee}[n_e(r)] - V_{xc}^{ee}[n_e^0] - \frac{1}{\beta} \int \tilde{C}_{Ie}(|\mathbf{r} - \mathbf{r}'|)(n_I(r') - n_I^0) d^3r', \quad (14)$$

where \tilde{C}_{Ie} is the non-Coulombic part of the direct ion-electron correlation function $C_{Ie}(r)$, which is defined by [30]

$$C_{Ie}(r) = \beta Z^*/r + \tilde{C}_{Ie}(r). \quad (15)$$

This new term is highlighted in yellow in Fig. 2. The second modification is that the ion density is described in terms of the ion-ion radial distribution function $g_{II}(r)$:

$$n_I(r) = n_I^0 g_{II}(r). \quad (16)$$

Whereas in the AA model $g_{II}(r)$ is chosen as a simple step function, here it is to be calculated on the basis of the Coulomb interactions in the plasma. As can be seen by comparing Figs. 1 and 2, the structure of the AA model remains unchanged except for the new contribution to $V_{Ne}^{\text{eff}}(r)$. The inputs to the model (Z, n_I^0, β) are the same and a criterion for μ_e^{id} must still be provided. In addition, closure of this modified AA model also requires $\tilde{C}_{Ie}(r)$ and $n_I(r)$ which can be calculated by coupling the AA model with a model of the plasma based on the Ornstein-Zernike integral equations theory of fluids [30]. The calculation of these two quantities increases the complexity of the problem considerably (Fig. 2).

3.1 Ornstein-Zernike integral equations theory of fluids and the two-component plasma model

Prior to the advances in computing power that allowed the direct simulation of classical fluids (Monte Carlo and Molecular Dynamics methods), the integral equations theory of fluids [44, 45] offered the most realistic description of an interacting fluid at a reasonable computing cost. It is the theory of choice to develop an AA model with correlations [27, 46, 28, 47, 26, 48, 30, 29].

The structure and thermodynamics of a fluid system of one type of classical point particles interacting via a pair potential is fully determined by its density n , temperature β and the pair potential $V(r)$. The most widely used integral equations theories of fluids are based on the Ornstein-Zernike equation

$$h(r) = C(r) + n \int C(|\mathbf{r} - \mathbf{r}'|) h(r) d^3 r'. \quad (17)$$

Expressed in Fourier space, Eq. (17) takes a simple form

$$h(k) = C(k) + nC(k)h(k), \quad (18)$$

where $F(k)$ denotes the Fourier transform of a function $F(r)$. The functions $h(r)$ and $C(r)$ are related to the pair potential by a closure relation

$$g(r) = h(r) + 1 = \exp(-\beta V(r) + h(r) - C(r) + B(r)). \quad (19)$$

In these equations, $g(r)$ is the pair distribution function, $h(r)$ is the pair correlation function, and $C(r)$ is the direct correlation function which is effectively defined by Eq. (17). Closing these two equations requires the knowledge of the bridge function $B(r)$ which accounts for n -body correlations beyond pair correlations. Various approximations to $B(r)$ are available [45]. Note that these relations are exact if the bridge function is known. Once the structure of the fluid (e.g. $g(r)$) is known, various quantities of interest, such as the thermodynamics can be calculated [44].

The above fluid equations can be readily generalized to mixtures of classical particles given the pair potentials $V_{ij}(r)$ between particles of type i and j [44, 45].

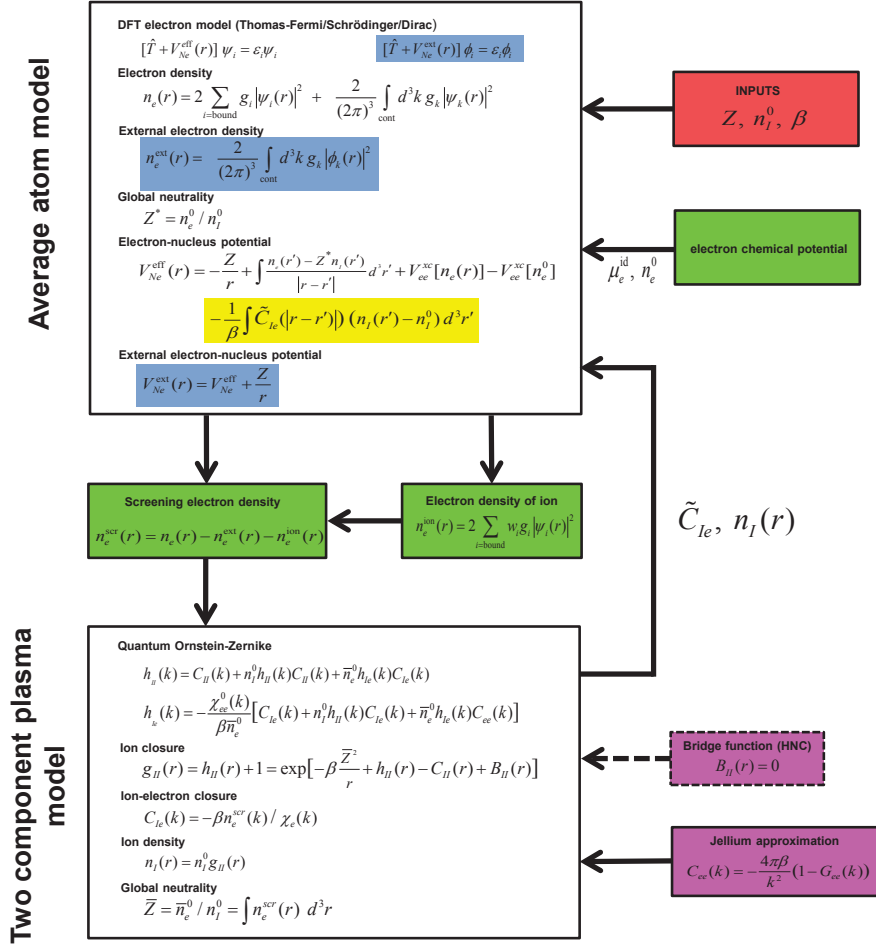


Fig. 2 Structure and key equations of the coupled average atom and two-component plasma model. The red box gives the input parameters to the model. Green boxes show elements where other choices are possible. Approximations are shown within purple boxes, with the dotted box indicating an approximation that can readily be improved. Arrows show the flow of information between the elements of the model. See text for details.

Chihara [49] has shown that the Ornstein-Zernike equation can be further generalized for a plasma of classical ions of density n_I^0 and quantum electrons of density \bar{n}_e^0

$$h_{II}(k) = C_{II}(k) + n_I^0 h_{II}(k) C_{II}(k) + \bar{n}_e^0 h_{Ie}(k) C_{Ie}(k) \quad (20)$$

$$h_{Ie}(k) = \frac{-\chi_{ee}^0(k)}{\beta \bar{n}_e^0} [C_{Ie}(k) + n_I^0 h_{II}(k) C_{Ie}(k) + \bar{n}_e^0 h_{Ie}(k) C_{ee}(k)] \quad (21)$$

where $\chi_{ee}^0(k)$ is the Lindhard response function of the non-interacting quantum electron gas. The quantum nature of the electrons is embodied in the factor $-\chi_{ee}^0(k)/\beta \bar{n}_e^0$. In the limit of a classical electron gas, this factor becomes unity and the classical Ornstein-Zernike equations are recovered. The ion closure relation has the same form as in the one component case

$$g_{II}(r) = h_{II}(r) + 1 = \exp\left(-\beta \frac{\bar{Z}^2}{r} + h_{II}(r) - C_{II}(r) + B_{II}(r)\right) \quad (22)$$

where the pair interaction is a pure Coulomb potential between ions of charge \bar{Z} .³ Global neutrality requires that

$$\bar{Z} = \bar{n}_e^0 / n_I^0. \quad (23)$$

The last four equations contain seven unknowns: \bar{Z} , h_{II} , h_{Ie} , C_{II} , C_{Ie} , C_{ee} and B_{II} . The closing of this system of equations will allow a solution that provides \tilde{C}_{Ie} (from Eq. 15) and $n_I(r) = n_I^0 g_{II}(r)$ that are needed to close the AA model with ion correlations (Fig. 2). The full set of equations will define a model that we will call a ‘‘two-component plasma’’ (TCP) model,

To close the equations of the TCP model, we start by introducing two approximations (purple boxes in Fig. 2). First, the bridge function is assumed to be $B_{II}(r) = 0$. This is the well-known hyper-netted chain (HNC) approximation to the Ornstein-Zernike integral equations theory of fluid (dashed purple box in Fig. 2). A better approximation is to use the bridge function of a similar interacting system that is more easily calculated than that of a general TCP. The bridge functions of the hard sphere fluid [50, 51], of the one-component plasma model [52], or for Yukawa systems [53], or bridge functions optimized with a variational approach [54] have all been used to model plasmas with the integral equations theory of fluids. For simplicity, and with good accuracy for the systems considered here (see §4), we will use the HNC approximation. The second approximation is to assume that the direct electron-electron correlation function C_{ee} is given by

$$C_{ee}(k) = \frac{-4\pi\beta}{k^2} (1 - G_{ee}(k, \beta, \bar{n}_e^0)) \quad (24)$$

where $G_{ee}(k, \beta, \bar{n}_e^0)$ is the local field correction of the jellium model. The jellium approximation (Eq. 24), to which there appears to be no reasonable alternative at this time, implies that the e - e correlations are decoupled from the ions. This is

³ Note that this is different from the AA ion charge Z^* , which is further discussed in §3.2.

reasonable as C_{ee} represent the correlations between unbound electrons. As long as the ion-electron correlations are not too strong, Eq. (24) is a good approximation. On the other hand, it would be a very poor approximation to describe bound electrons which are intrinsically very strongly correlated with the ions.

One additional equation is needed to close the TCP model, which is to be provided by the AA model (downward arrows in Fig. 2). This closure will also determine the charge of the ion \bar{Z} and thus the direct ion-ion potential in the TCP model. This closure is not unique, however [48, 30, 27, 28], and is illustrated with the green boxes in Fig. 2. We found that the most satisfactory approach is to use the solution of the AA model to calculate the electron density that screens an individual ion in the plasma. The AA model is naturally suited for this purpose as it is designed to calculate the properties of a single ion in a plasma. This screening electron density is defined in two steps.

In the first step, the electron density profile $n_e(r)$ obtained from the AA model is separated into a contribution that is assigned to a single nucleus (defining a ‘‘pseudo-atom’’ [55, 56, 28]) and an external contribution, due to the electrons in the surrounding plasma. The separation is effected by solving the AA model a second time after removing the central nucleus from the effective electron-nucleus potential $V_{Ne}^{\text{eff}}(r)$, keeping everything else fixed. The resulting electron density is thus computed only from the field of the surrounding plasma $V_{Ne}^{\text{ext}}(r)$ and defines the external electron density $n_e^{\text{ext}}(r)$. The AA equations corresponding to this external system are shown in blue boxes in Fig. 2. Note that in the absence of the central nucleus, the potential $V_{Ne}^{\text{ext}}(r)$ is repulsive almost everywhere and does not support bound states. This pseudo-atom electron density is $n_e^{\text{PA}}(r) = n_e(r) - n_e^{\text{ext}}(r)$.

The second step consists of extracting from $n_e^{\text{PA}}(r)$ the part that will define (along with a central nucleus) an ion, and the remainder which is to be assigned to the electron fluid of the plasma. The most straightforward separation is to assign the bound electrons to the ion and the continuum electrons to the TCP electron fluid. This definition of an ion for the TCP model (green box in Fig. 2) is by no means unique. For instance, the density in the neighborhood of the nucleus associated with continuum resonances of low energy is qualitatively similar to the electron density of a weakly bound state. Thus, it would be reasonable to count those resonant electrons as part of the ion. Such an approach was suggested by Chihara [27] but is not satisfactory in practice as it requires additional arbitrary criteria to determine which resonances should be considered part of the ion and to separate the electron density associated with a resonance from the background continuum electrons.

This simple definition of the ion electron cloud is not without drawbacks. Most flagrant is that the electron density of the bound states is a discontinuous function of n_I^0 when a state crosses into the continuum of positive energies, i.e. when it is pressure-ionized, a phenomenon of great importance in studies of WDM. As a consequence, every quantity appearing in the model becomes discontinuous with density. This can be avoided by applying occupation factors $0 \leq w_i(r) \leq 1$ in the sum

$$n_e^{\text{ion}}(r) = 2 \sum_{i=\text{bound}} w_i(r) g_i |\psi_i(r)|^2 \quad (25)$$

which are calculated from a simple model for the broadening of the bound energy levels [30]. As a weakly bound, broadened level starts to cross into the continuum of positive energies, $w_i(r)$ decreases below unity and vanishes once $\varepsilon_i = 0$. Furthermore, $w_i(r)$ includes a smooth radial cutoff that damps the tails of weakly bound states that extend far from the central nucleus [28, 30]. Physically, this accounts for the fact that the bound electron density that is located far from the nucleus cannot be assigned to the central ion in the presence of the other neighboring ions. This cut-off also resolves a numerical difficulty with the spatial integration of long-ranged functions. With these elements it is now possible to define the screening electron density

$$n_e^{\text{scr}}(r) = n_e(r) - n_e^{\text{ext}}(r) - n_e^{\text{ion}}(r). \quad (26)$$

This is the density of electrons that are associated with the central nucleus but are “free”, i.e. not part of the central ion. These electrons respond to the attractive field of the ion, screening the ion-ion interaction. From the quantum OZ equations, it can be shown [46, 27, 30] that the response of the electron fluid gives the screening density in terms of direct correlation functions

$$n_e^{\text{scr}}(k) = -\chi_{ee}(k)C_{Ie}(k)/\beta \quad (27)$$

where

$$\chi_{ee}(k) = \frac{\chi_{ee}^0(k)}{1 + \chi_{ee}^0(k)C_{ee}(k)/\beta} \quad (28)$$

is the response function of the correlated quantum electron fluid [57]. Equation (27) has the form of a linear response of the electron fluid to an external pseudo-potential $-C_{Ie}/\beta$. However, in this case the response is highly non-linear since $n_e^{\text{scr}}(r)$ is calculated from the solution of the Schrödinger equation rather than linear response theory. Inverting Eq. (27) gives

$$C_{Ie}(k) = -\beta n_e^{\text{scr}}(k)/\chi_{ee}(k) \quad (29)$$

which is an exact relation within the TCP model. Furthermore, global neutrality of the TCP plasma requires that the ion charge \bar{Z} be related to the screening density by

$$\bar{Z} = \bar{n}_e^0/n_I^0 = \int n_e^{\text{scr}}(r) d^3r. \quad (30)$$

By taking n_e^{scr} defined from the AA model (Eq. 26), we now have the final equation required to close the TCP model, which provides \tilde{C}_{Ie} (Eq. 15) and $n_I(r)$ that in turn close the AA model (Fig. 2). The two sets of equations are solved iteratively between the AA and TCP models.

Thus, the coupling between the AA and the TCP models is provided by defining a screening density from a solution of the Schrödinger equation for the Z electrons belonging to the central nucleus in the AA model. This particular choice is not unique (hence the green box in Fig. 2). In the same spirit, the Quantum Hypernetted-Chain (QHNC) model of Chihara [27, 46], couples the AA and TCP models in terms of the pair correlation function

$$n_e^0 h_{Ie}(r) = n_e^f(r) - n_e^0 \quad (31)$$

where $n_e^f(r)$ is the density of continuum electrons (second term in Eq. 4). Like Eq. (29), this choice for the coupling relates a quantity associated with the density of free electrons obtained in the AA model (n_e^f instead of n_e^{scr}) to a correlation function in the TCP model (h_{Ie} instead of C_{Ie}). The QHNC closure has the drawback that $n_e^0 = \bar{n}_e^0$, i.e. $\bar{Z} = Z^*$, which overly constrains the model, as we will see below.

The electron chemical potential (green box in Fig. 2) is given as in the AA model (Eq. 9), with a step function $g_{II}(r)$. This is inconsistent with the pair distribution function obtained in the TCP model but is numerically advantageous and, given the ambiguous nature of the local neutrality condition, is very reasonable. Other choices include imposing charge neutrality as in Eq. (9) but over a correlation sphere of radius $R_c > R$ [47], or $Z = N_b + n_e^0/n_I^0$ as in several AA models.

This completes the formulation of the self-consistent model for an average atom embedded in a plasma of correlated ions. This AA+TCP model assumes spherical symmetry and consists of an AA model coupled to a TCP model based on the Ornstein-Zernike integral equations theory of interacting fluids. A screening electron density is calculated within the AA model to obtain an ion-electron correlation function for the TCP model, which in turns provide correlation functions for the AA atom model. The model has no adjustable parameters and only needs the nuclear charge, ion density and temperature as inputs. It formally recovers the classical one-component plasma model (OCP) [58] and the screened one-component plasma model (SOCP) [59]. The solution of the closed system of equations gives all the pair correlation functions between ions and electrons, the effective ion-ion and nucleus-electron pair potentials, the bound and continuum wave functions and eigenvalues, the ion charge, and the electron densities. These quantities, some of which are directly amenable to experimental measurements, form the basis upon which WDM properties of interest, such as the equation of state, conductivities, and opacities can be calculated.

3.2 The role of plasma correlations

The role of ion-ion correlations in the AA+TCP model is revealed by comparing some key model quantities calculated with an imposed, step function pair distribution function $g_{II}(r)$ (Eq. 8) as in a typical AA model and with the full self-consistent $g_{II}(r)$ from the AA+TCP model. For clarity, we will call the former the jellium vacancy model (JVM).⁴ These results are shown in Figs. 3 – 6 for the case of Al at $T = 1 \text{ eV}$ (0.0367 Ha) and $\rho = 2.7 \text{ g/cm}^3$ (solid density). Under these conditions, the ions are strongly correlated and $g_{II}(r)$ shows much structure which is only crudely approximated by the step function ion distribution of the JVM (Fig. 3).

The effect of the ion correlations on the effective nucleus-electron potential $V_{Ne}^{\text{eff}}(r)$ that enters the Schrödinger equation of the AA model is shown in Fig. 4.

⁴ This is the same model as the JVM of [18] and similar to the JVM of [27].

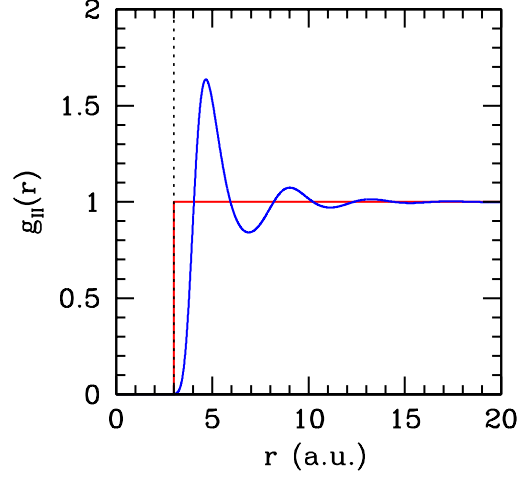


Fig. 3 Pair distribution functions of the JVM model (red) and the AA+TCP model (blue) for Al at $T = 1$ eV and $\rho = 2.7$ g/cm³. At this density, the ion sphere radius is $R = 2.99$ a.u., which is indicated by a dotted line.

At this density, the $1s^2$, $2s^2$ and $2p^6$ electrons of Al are tightly bound (our model predicts binding energies of -54.6, -3.4 and -2.0 Ha, respectively, measured from the bottom of the valence band) and confined to $r \lesssim 2$ a.u. (see below). Thus the core electrons are not sensitive to the difference in $g_{II}(r)$ and the two potentials are identical in the core. Both show a small positive maximum at $r \sim R$ as the central “ion hole” (Fig. 3) amounts to a repulsive contribution to the effective nucleus-electron potential. Differences, which can be as large as 0.02 Ha (0.5 eV), are mainly confined to $R \lesssim r \lesssim 3R$, as is expected from the difference in the ion-ion distribution function (Fig. 3). At this relatively low temperature, $V_{Ne}^{\text{eff}}(r)$ has Friedel oscillations at large r superimposed on the effect of decaying oscillations in $g_{II}(r)$. Both go away at higher T [30, 60].

In the TCP model, an effective ion-ion pair potential that takes into account the electron screening can be defined [30, 46, 27]

$$\beta V(k) = \beta \frac{4\pi\bar{Z}^2}{k^2} - n_e^{\text{scr}}(k)C_{Ie}(k). \quad (32)$$

The first term is the repulsive Coulomb potential between two point ions of charge \bar{Z} and the second term is the screening (mainly attractive) potential from the surrounding electrons that ensures that $V(r)$ is short-ranged. This effective ion-ion potential is plotted in Fig. 5 as $rV(r)$. The ion charge is $\bar{Z} = 3$ and a pure Coulomb potential would appear as a flat line at $rV(r) = 9$. The ion-ion potential reaches this limit as

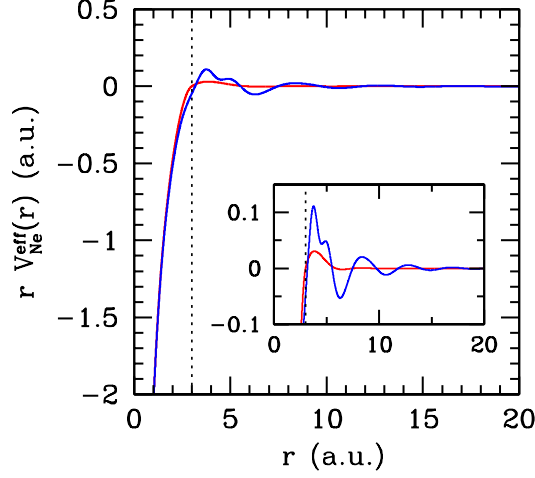


Fig. 4 Effective nucleus-electron potential for the JVM (red) and the AA+TCP model (blue), from Eqns. (3) and (14), respectively, for the same conditions as in Fig. 3. The inset magnifies the behavior at larger r . The product $rV_{Ne}^{eff}(r)$ is plotted for clarity and the dotted line indicates the ion sphere radius $R = 2.99$ a.u..

$r \rightarrow 0$. Strong screening of the ion charge is evident as $rV(r)$ decreases rapidly to very small values within $\lesssim 2R$. The potential shows two small bumps at $r \sim 0.07$ and 0.85 a.u. that are associated with minima in $n_e^{scr}(r)$ (see below). This is consistent with Poisson's equation for the electrostatic contribution of n_e^{scr} to the ion-ion potential. Small oscillations outside the ion sphere (inset) are caused by the structure in $g_{II}(r)$.

The various electron densities that appear in the model, $n_e(r)$, $n_e^{ext}(r)$, $n_e^{PA}(r)$, $n_e^{ion}(r)$ and $n_e^{scr}(r)$ are shown in Fig. 6. At the scale of this figure, these electron densities are nearly identical when computed with either the JVM or the AA+TCP model. Only the latter are shown for clarity. The total electron density $n_e(r)$ (Eq. 4, blue curve) shows two peaks within 1 a.u. that correspond to the $1s^2$ and the $2s^2 2p^6$ bound electrons. The continuum electrons that are attracted to the nucleus and its bound electrons cause an excess of density near the ion sphere radius. At large r , $n_e(r) \rightarrow n_e^0$ and $4\pi r^2 n_e(r)$ diverges as r^2 . The electron density associated with the plasma external to the central nucleus, $n_e^{ext}(r)$ (black curve) is similar to $n_e(r)$ except that it does not support bound states and has no build up of screening charge. The difference between these two electron densities defines the electron cloud associated with the central nucleus, i.e. a pseudo-atom $n_e^{PA}(r) = n_e(r) - n_e^{ext}(r)$ (green curve), which is essentially confined within $\sim 2R$. The ion electron cloud ($n_e^{ion}(r)$) is defined as the density that arises from the bound states (Eq. 25; red curve) which shows peaks associated with the K and L shells. Finally, the electron

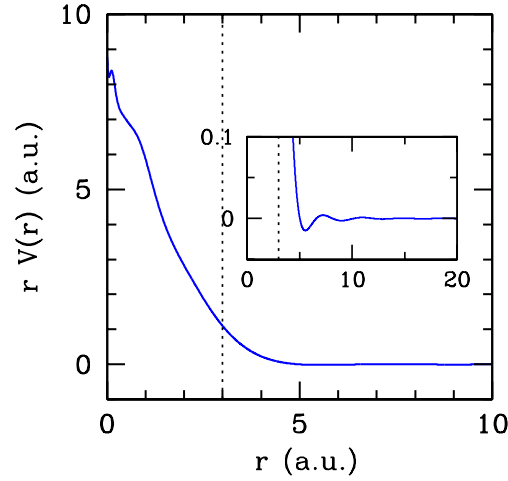


Fig. 5 Effective ion-ion potential in the the AA+TCP model, given by Eqn.(32) for the same case as in Fig. 3. The inset magnifies the behavior at larger r . The ion sphere radius $R = 2.99$ a.u. is shown by the dotted line. The product $rV(r)$ is plotted for clarity.

density that couples the AA and TCP model (Fig. 2 and Eq. 29) is the screening density $n_e^{\text{scr}}(r) = n_e^{\text{PA}}(r) - n_e^{\text{ion}}(r)$ (cyan curve). It forms a broad peak outside of the core states that decays rapidly beyond the ion sphere radius. This results from the attractive force of the net positive charge of the ion (nucleus + bound states), the repulsion from the bound electrons and the orthogonality of the continuum and bound states. Details of $n_e^{\text{scr}}(r)$ are shown in the lower panel of Fig. 6.

It turns out that by running the electron densities obtained with the JVM through a single pass of the TCP model (without requiring the self-consistency, see Fig. 2) gives distribution functions that are good approximations to the fully converged solutions [30]. This realization has been a key element of the successful numerical implementation of the model as it substantially improves the convergence. It also implies that approximate but fairly good $g_{II}(r)$ for the AA+TCP model can be calculated at very little computational cost above that of the JVM model.

As pointed out above, the ion charge in the AA part of the model, Z^* , and in the TCP part of the model, \bar{Z} are two distinct quantities, as are the corresponding free electron densities, n_e^0 and \bar{n}_e^0 . It should be clear from Fig. 2 that we are coupling two different models and that mathematically it is not required that these ion charges be equal. In fact, they are quite different, as can be seen in Fig. 7. As expected, the ion charge increases steadily with temperature. The counterintuitive distinction between \bar{Z} and Z^* can be understood physically as follows. In the AA model, n_e^0 is the density of electrons in the field-free region of space ($V_{Ne}^{\text{eff}} = 0$), far from the central nucleus, which has a clear meaning within a model with a single central nucleus embedded

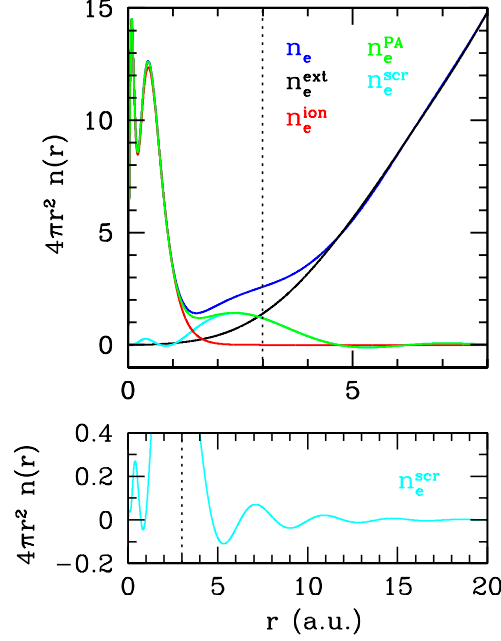


Fig. 6 Electron densities for Al at $T = 1$ eV and 2.7 g/cm 3 . Only the electron densities from the AA+TCP model are shown for clarity. The total electron density (Eq. 4) is in blue, and the density from the system external to the ion (i.e. without the central nucleus) n_e^{ext} is in black. The difference between them is the pseudo-atom density $n_e^{\text{PA}} = n_e - n_e^{\text{ext}}$, which represent the Z electrons, bound and unbound, associated with the central nucleus (green). The density of electrons which, along with the central nucleus, define an ion is n_e^{ion} (Eq. 25, red). Finally, the screening density $n_e^{\text{scr}} = n_e^{\text{PA}} - n_e^{\text{ion}}$ is shown in cyan. The lower panel, which is on different scale, shows the smaller structure of n_e^{scr} . In the upper panel, the n_e and n_e^{ext} curves diverge as r^2 at large r because both densities become constant and the figure shows the densities multiplied by $4\pi r^2$. The vertical dotted line shows the ion sphere radius $R = 2.99$ a.u.

in a spherically averaged plasma. In the TCP model, on the other hand, \bar{n}_e^0 represents the density of the inhomogeneous electron fluid (made up of those electrons that are not included in the ions), averaged over all space. This corresponds more closely to the concept of the electron density in a real dense plasma, where there is no field-free region as an electron always finds itself in the field of some nearby ion(s). Thus, the free electron density in the AA model (n_e^0) is a rather artificial construct that arises from the simplifying concept that the electronic structure around a central nucleus in a smeared out plasma is a good approximation for the “average” electronic structure in a correlated, multi-center plasma. Within the AA+TCP model, the physical electron density (to be used in a conductivity calculation, for example) is \bar{n}_e^0 , with corresponding ion charge \bar{Z} . This is confirmed in Fig. 7 where $\bar{Z} \rightarrow 3$ at low T , which is the number of valence electrons of Al under normal con-

ditions. On the other hand, $Z^* \sim 2$ at low T , which would be a poor estimate of the valence electron density in normal aluminum, should it be (wrongly) interpreted as such.

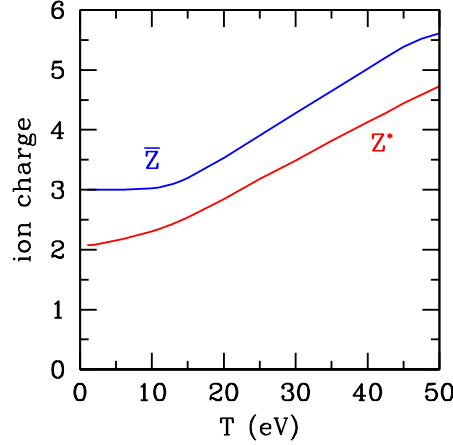


Fig. 7 Ion charge as a function of temperature for solid density Al (2.7 g/cm^3). The ion charge from the coupled average atom Z^* and the two-component plasma models \bar{Z} are shown. The roles of \bar{Z} and Z^* are illustrated in Fig. 2.

3.3 Appraisal of the model

Given the theoretical development and numerical solutions of the model outlined above, it is possible to ascertain its advantages and limitations at a semi-quantitative level. There are several advantages over computer simulations of WDM. Most immediate is the substantial economy of computer time to converge to a solution. Depending on the temperature and density, the solution of the AA+TCP model is typically 2 to 3 orders of magnitude faster than a QMD simulation. Computer simulations are inherently subject to statistical noise (fluctuations) due to the finite number of particles considered. The finite size of the simulation box limits spatial sampling of the system, such as the radial extent over which the pair distribution function can be evaluated (Figs. 8 – 9). On the other hand, the AA+TCP model consists of coupled algebraic, differential and integral equations whose solution is smooth within the numerical accuracy of the algorithms. The equations are solved over a comparatively large computational volume of typically 10–20 times the ion sphere radius, which effectively corresponds to an infinite system. It also treats all of the elec-

trons explicitly and on the same footing. There is no pseudo-potential or concern about their transferability. The model gives good solutions over a range of temperatures and densities that is much broader than the typical range of applicability of any one *ab initio* method. It is also worth noting that a version of the model where the Schrödinger equation is replaced by the semi-classical Thomas-Fermi model of the electrons gives viable results even for strongly coupled systems [30], contrary to the conclusions of an earlier effort to develop a Thomas-Fermi AA model with ion-ion correlations [29]. Furthermore, the quantum mechanical version recovers the Thomas-Fermi results in the high-density, high-temperature limit [30]. This is a valuable internal check on the physics and numerical implementation of the model.

While these are significant advantages over *ab initio* simulations of WDM, the model does not fare as well in other aspects. The substantial savings of computer time come at the cost of more approximate physics. In particular, the model only considers pair interactions and is restricted to spherical symmetry. It cannot account for chemical bonding or angular forces. Its range of validity has been demonstrated to be quite broad in terms of T , ρ and Z , which shows promise for its usefulness to many potential applications, but its limits have not yet been established. It is worth pointing out that the AA model, like QMD, is based on the finite temperature DFT formalism, and thus both methods share the limitations associated with this approach (such as the well-known underestimation of the electronic band gap, approximate energies for the bound states, the fictitious nature of the unoccupied states, etc).

Perhaps of more concern are the elements of the model that readily admit other possible choices (green boxes in Fig. 2). This introduces a level of arbitrariness in the model whose effect on the solution is not negligible but has not been quantified. Our choices have been guided by earlier work, our understanding of the AA and TCP models, and the pragmatic need for a stable numerical solution of the system of equations. Nonetheless, the choices adopted are reasonable and their validity can be established by assessing the accuracy of the results.

4 Results: Pair distribution functions

A converged solution of the system of equations that define the model consists of the electronic wave functions and energies of bound states, the continuum wave functions including resonances, the ion-ion and nucleus-electron effective potentials, the average ion charge, and all the correlation and distribution functions that describe the structure of the two component ion-electron fluid. Of all these quantities, the ion-ion pair distribution function $g_{II}(r)$ is the most readily amenable to a comparison with experimental data and computer simulations. The experimental measurement of the structure of WDM is in its infancy and very sparse [5, 6] but a number of results from *ab initio* simulations are available. All the calculations shown in this section were performed in the HNC approximation where $B_{II}(r) = 0$. This approx-

imation is expected to become gradually worse as the ion-ion coupling increases such as at lower temperatures or higher ionic densities.

The pair distribution function of aluminum at solid density (2.7 g/cm^3) and temperatures from 1 to 15 eV is compared to the results of QMD simulations [60] in Fig. 8. The agreement is essentially perfect at $T = 2 \text{ eV}$ and above and remains very good at 1 eV where deviations likely due to the HNC approximation are discernible. We emphasize that this excellent agreement is not the result of a fit as there is no adjustable parameter in the AA+TCP model.

For metals around solid density, QMD simulations become computationally impractical when the temperature is comparable to or larger than the Fermi temperature, which typically puts an upper bound of $\sim 10 - 20 \text{ eV}$ on the applicability of the method. However, the method can be extended to higher T by using the semi-classical Thomas-Fermi model of the electrons rather than a quantum model. Such Thomas-Fermi Molecular Dynamics (TFMD) calculations have been performed along the principal Hugoniot of iron up to 5000 eV [22] over compression ratios ρ/ρ_0 of 2.9 to 5.0. For this comparison (Fig. 9) we ran the AA+TCP model with the Thomas-Fermi model of the electrons. At $T = 10 \text{ eV}$ and 22.5 g/cm^3 , both calculations include electron exchange and agree perfectly. The agreement remains excellent at the three higher Hugoniot points. For the latter, the TFMD calculations do not include electron exchange; a contribution that should diminish rapidly as T increases. The small shift in the highest temperature point (5000 eV) for $r/R \lesssim 1$ is somewhat puzzling given the lower ion-ion coupling and the excellent agreement at 1000 eV. On the other hand, a calculation with the screened one-component plasma model (SOCP [59]), which uses linear response theory to describe the electron screening, is in perfect agreement with our $g_{II}(r)$ at $T = 5000 \text{ eV}$ (not shown, as the curves are indistinguishable on the scale of the figure). This suggests that the departure with the TFMD simulation at this very high temperature may be revealing some statistical inaccuracy in the latter, as suggested by the growing level of noise in the simulations as T increases. The same calculations with the *quantum* AA+TCP give $g_{II}(r)$ that are identical to the Thomas-Fermi results [30], with only small differences appearing at 10 eV. Thus the quantum version of the model recovers the Thomas-Fermi limit at high T and high ρ .

Finally, the $g_{II}(r)$ of very dense hydrogen (80 g/cm^3), or about 800 times the solid density) is found to agree perfectly (within the scatter) with QMD simulations [62] at $T = 172 \text{ eV}$ and to match very well the QMD result at 5 eV (Fig. 10). Again, a calculation with the linear response SOCP model gives an identical $g_{II}(r)$ as with the AA+TCP model (not shown). This demonstrates that in the limit of weak electron-ion coupling (but moderate to strong coupling and electron degeneracy), the quantum AA+TCP model recovers the proper limit of linear screening.

While the model must be tested more extensively, several important points can already be made:

1. The numerical solution of the model's equations has been successfully implemented and convergence achieved for a wide range of warm and hot dense matter conditions ($Z=1-26$, $T = 1 - 5000 \text{ eV}$, $\rho/\rho_0 = 1 - 800$).

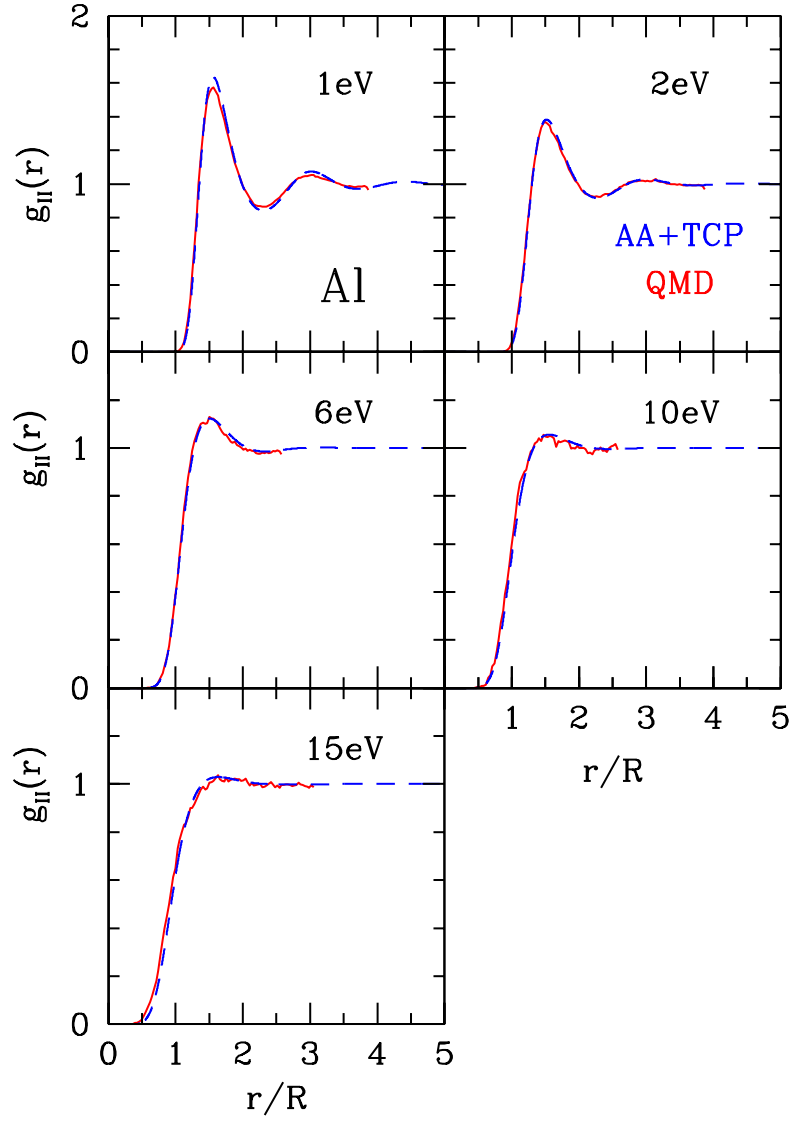


Fig. 8 Pair distribution function of aluminum at solid density (2.7 g/cm^3) and five temperatures ranging from 1 to 15 eV. The red curves are quantum molecular dynamics (QMD) simulations [60]. The results of the AA+TCP model are shown in blue. R is the ion sphere radius (Eq. 1) which is 2.99 a.u. in all cases shown. Note that the last three panels are on a different vertical scale.

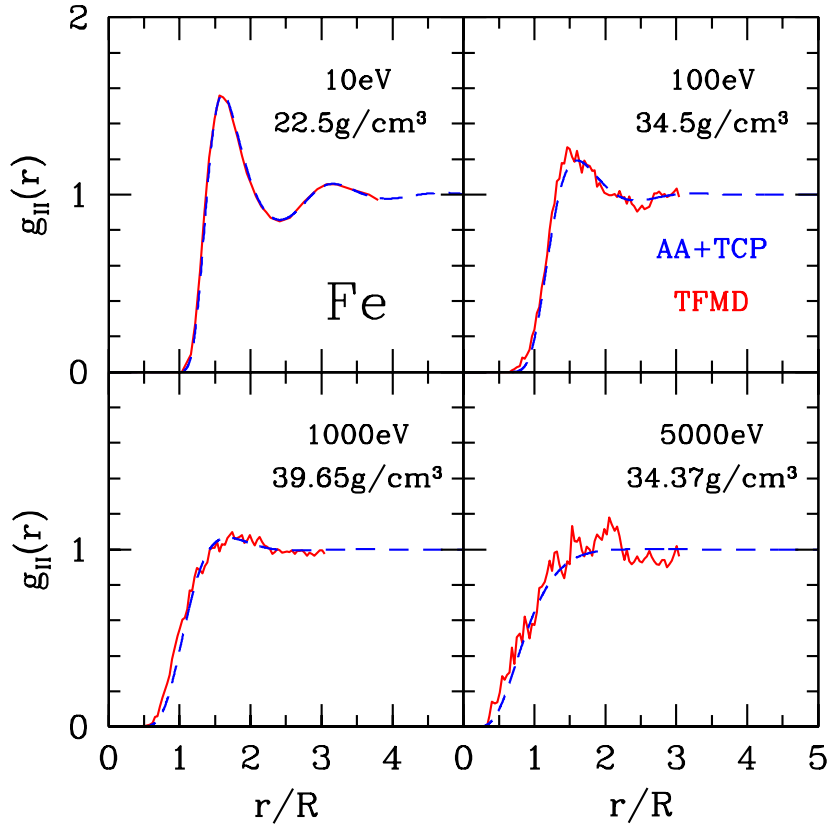


Fig. 9 Pair distribution function of iron for four (T, ρ) points along the principal Hugoniot. The red curves are Thomas-Fermi molecular dynamics (TFMD) simulations. The 10eV calculation includes electron exchange [61] while the other three (100 – 5000eV) do not [22]. The AA+TCP calculations (blue) were done with the Thomas-Fermi model of the electrons and all include exchange. R is the ion sphere radius (Eq. 1).

2. Excellent agreement is found in comparisons of the pair distribution function with QMD/TFMD simulations.
3. The AA+TCP model with quantum electrons recovers the results of the AA+TCP with the Thomas-Fermi model of the electrons in the high- T , high- ρ regime.
4. In the limit of weak ion-electron coupling, the quantum AA+TCP model recovers the SOCP model.
5. A Thomas-Fermi AA model with ion correlations can be successfully defined and implemented.

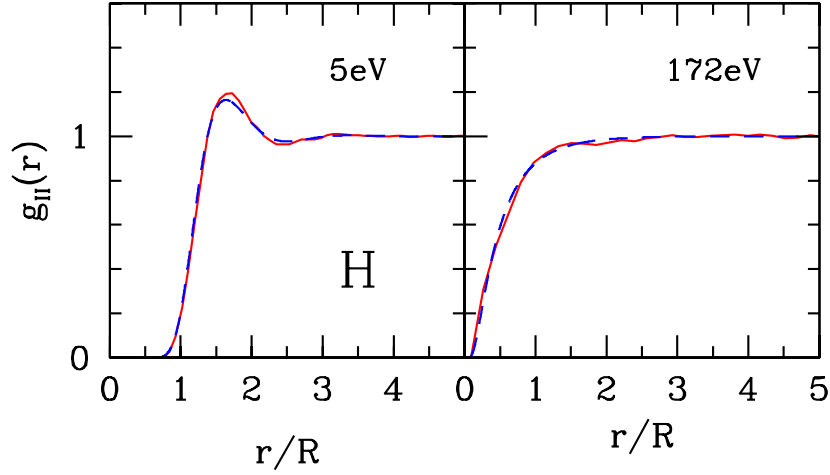


Fig. 10 Pair distribution function of hydrogen at 80 g/cm^3 and $T = 5$ and 172 eV . The red curves are quantum molecular dynamics (QMD) simulations [62]. The results of the AA+TCP model are shown in blue. $R = 0.323 \text{ a.u.}$ is the ion sphere radius (Eq. 1).

5 Summary and outlook

We have presented a model of warm dense matter that extends the popular average atom (AA) models by introducing the correlations in the surrounding plasma, which replaces a “one ion” description of WDM by one for the whole plasma. The plasma is a mixture of classical ions and quantum electrons described with the integral equations theory of interacting fluids, which we call a two-component plasma model (TCP). The AA and TCP models are coupled self-consistently, each providing quantities necessary to close the other. The electronic structure surrounding a nucleus takes into account Coulomb interactions with the surrounding plasma, whose ions and the response of the electron fluid (screening) are in turn described by the solution for the central ion. The resulting AA+TCP model has no free parameters and only requires the nuclear charge Z , the temperature T , and the ion density n_i^0 as inputs. The electrons can be treated semi-classically (Thomas-Fermi) or quantum mechanically (Schrödinger or Dirac equation). The form adopted for the coupling between the two models is original and leads to the recognition that the ion charge in the AA model is different from that in the TCP model. The latter is the physically relevant charge related to observables. Earlier AA models with plasma correlations did not recognize this point and were overly constrained.

The introduction of plasma correlations increases considerably the mathematical and numerical complexity of the model, which is mitigated by imposing spherical symmetry on the problem. The model was developed with an emphasis on for-

mal development, internal consistency, and well-defined approximations, which we think, has been achieved to the extent that is possible when combining an AA model with the integral equations theory of fluids. On the other hand, such a coupled model has intrinsic ambiguities that require some ad hoc choices, such as in the criterion for the ideal chemical potential of the electrons and the definition of which electrons are to be counted as part of an ion. These are the less satisfying features of the model. In principle, some of these choices must be better than others, something that can be established by comparison with other theories that are free of such ambiguities (e.g. computer simulations, expansions around a non-interacting plasma state) or with experiments.

So far, the model has been validated by comparing the ion-ion pair distribution function of a wide range of warm and hot dense matter systems with those calculated with *ab initio* simulations. The agreement is uniformly excellent. For cases where the linear response describes the electron fluid accurately, comparisons with the screened one-component plasma model show perfect agreement. In those cases, deviations with the TFMD *ab initio* simulations shown suggest that the latter may not be very accurate. The AA+TCP with a Thomas-Fermi model of the electrons is a viable model of hot dense matter. Finally, the AA+TCP model with quantum mechanical electrons recovers the AA+TCP model with the Thomas-Fermi model of the electrons at high densities and temperatures. The goal of developing a computationally efficient model has been achieved: Each of the results shown in Figs. 8–10 runs in about one hour on a single processor workstation.

The realism of the AA+TCP model can be improved in several ways without modifying its structure (Fig. 2) or changing the key assumptions. Foremost is introducing an ion-ion bridge function which will extend the accuracy of the model to low temperatures where the coupling is very strong (e.g. liquid metals). Other possible refinements include the core overlap interaction in the direct ion-ion potential, relativity (Dirac equation), and a more sophisticated exchange and correlation potential, such as a generalized gradient approximation functional.

Computer simulation methods combine theory and sophisticated algorithms to calculate the microscopic properties of dense plasmas. The AA+TCP is a different approach that provides nearly all of the same microscopic properties. Both methods can be thought of as “central engines” around which the calculation of many macroscopic properties of WDM can be built. The AA+TCP model can thus form the basis for the calculation of nearly all the quantities typically obtained with computer simulations such as thermodynamics, conductivity, opacities, diffusion coefficients, and viscosity. It can be applied to the analysis of X-Ray Thomson scattering (XRTS) experiments as well as X-ray absorption near-edge spectroscopy (XANES) experiments. Furthermore, the model can be readily expanded to treat mixtures of ions without any additional approximation or assumption. Here the AA+TCP model offers a distinct advantage over simulations as it can model highly asymmetric and very dilute mixtures.

This new average atom model with plasma correlations has so far shown a very satisfactory degree of physical realism. It is a significant step beyond the more common “atom in a cell” models of warm dense matter. In view of its relatively modest

computational cost and its many potential applications, it is a promising approach to produce extensive tabulations of warm dense matter properties.

Acknowledgements We gratefully acknowledge V. Recoules, F. Lambert, J. D. Kress and L. Collins for providing pair distribution functions from their *ab initio* simulations. This work was performed under the auspices of the United States Department of Energy under contract DE-AC52-06NA25396.

References

1. Report of ReNew workshop, *Basic research needs for high energy density laboratory physics* (U.S. Department of Energy, 2009). <http://science.energy.gov/media/fes/pdf/workshop-reports/hedlp-brn-workshop-report-oct-2010.pdf>
2. A.W. DeSilva, J.D. Katsouras, Phys. Rev. E **57**, 5945 (1998)
3. A. Mančić, *et al.*, Phys. Rev. Lett. **104**, 035002 (2010)
4. J. Eggert, S. Brygoo, P. Loubeyre, R.S. McWilliams, P.M. Celliers, D.G. Hicks, T.R. Boehly, R. Jeanloz, G.W. Collins, Phys. Rev. Lett. **100**, 124503 (2008)
5. E.G. Saiz, *et al.*, Nature physics **4**, 940 (2008)
6. A.L. Kritcher, *et al.*, Science **322**, 69 (2008)
7. O. Ciricosta, *et al.*, Phys. Rev. Lett. **109**, 065002 (2012)
8. A. Benuzzi-Mounaix, F. Dorchies, V. Recoules, F. Festa, O. Peyrusse, A. Lévy, A. Ravasio, T. Hall, M. Koenig, N. Amadou, E. Brambrink, S. Mazevet, Phys. Rev. Lett. **107**, 165006 (2011)
9. F. Dorchies, A. Lévy, C. Goyon, P. Combis, D. Descamps, C. Fourment, M. Harmand, S. Hulin, P.M. Leguay, S. Petit, O. Peyrusse, J.J. Santos, Phys. Rev. Lett. **107**, 245006 (2011)
10. T. Ma, T. Döppner, R.W. Falcone, L. Fletcher, C. Fortmann, D.O. Gericke, O.L. Landen, H.J. Lee, A. Pak, J. Vorberger, K. Wünsch, S.H. Glenzer, Phys. Rev. Lett. **110**, 065001 (2013)
11. T. Guillot, D.J. Stevenson, W.B. Hubbard, D. Saumon, *Jupiter – The planet, Satellites and Magnetosphere* (University of Arizona Press, 2005), chap. 3
12. R. Redmer, T.R. Mattsson, N. Nettelmann, M. French, Icarus **211**, 798 (2011)
13. G. Fontaine, H.M.V. Horn, Astrophys. J. Supp. **31**, 467 (1976)
14. J.J. Fortney, S.H. Glenzer, M. Koenig, B. Militzer, D. Saumon, D. Valencia, iPhys. Plasmas **16**, 1003 (2009)
15. D.A. Liberman, J. Quant. Spectros. Radiat. Transfer **27**, 335 (1982)
16. B. Wilson, V. Sonnad, P. Sterne, W. Isaacs, J. Quant. Spectros. Radiat. Transfer **99**, 658 (2006)
17. P. Sterne, S. Hansen, B. Wilson, W. Isaacs, High Energy Density Physics **3**, 278 (2007)
18. R. Piron, T. Blenski, Phys. Rev. E **83**, 026403 (2011)
19. S. Mazevet, M.P. Desjarlais, L.A. Collins, J.D. Kress, N.H. Magee, Phys. Rev. E **71**, 016409 (2005)
20. M.P. Desjarlais, J.D. Kress, L.A. Collins, Phys. Rev. E **66**, 025401(R) (2002)
21. G. Zérah, J. Clérouin, E.L. Pollock, Phys. Rev. Lett. **69**, 446 (1992)
22. F. Lambert, J. Clérouin, G. Zerah, Phys. Rev. E **73**, 016403 (2006)
23. D.M. Ceperley, Rev. Mod. Phys. **67**, 279 (1995)
24. K.P. Driver, B. Militzer, Phys. Rev. Lett. **108**, 115502 (2012)
25. B. Holst, R. Redmer, Phys. Rev. B **77**, 184201 (2008)
26. H. Xu, J.P. Hansen, Phys. Rev. E **57**, 211 (1998)
27. J. Chihara, J. Phys: Condens. Matter **3**, 8715 (1991)
28. F. Perrot, Phys. Rev. E **47**, 570 (1993)
29. D. Ofer, E. Nardi, Y. Rosenfeld, Phys. Rev. A **38**, 5801 (1988)
30. C.E. Starrett, D. Saumon, Phys. Rev. E **87**, 013104 (2013)

31. W. Kohn, L.J. Sham, Phys. Rev. **140**, A1133 (1965)
32. N.D. Mermin, Phys. Rev. **137**, A1441 (1965)
33. R. Parr, W. Wang, *Density functional theory of atoms and molecules* (Oxford University Press, 1989)
34. L.H. Thomas, Proc. Camb. Phil. Soc. **23**, 542 (1927)
35. E. Fermi, Zeits. Phys. **48**, 73 (1928)
36. R.P. Feynman, N. Metropolis, E. Teller, Phys. Rev **75**, 1561 (1949)
37. T. Blenski, B. Cichocki, Phys. Rev. E **75**, 056402 (2007)
38. D.A. Liberman, Phys. Rev. B **20**, 4981 (1979)
39. T. Blenski, K. Ishikawa, Phys. Rev. E **51**, 4869 (1995)
40. E. Wigner, F. Seitz, Phys. Rev. **43**, 804 (1933)
41. B.J.B. Crowley, J.W. Harris, J. Quant. Spectros. Radiat. Transfer **71**, 257 (2001)
42. B.F. Rozsnyai, Phys. Rev. A **5**, 1137 (1972)
43. G. Faussurier, C. Blancard, P. Cossé, P. Renaudin, Phys. of. Plas. **17**, 052707 (2010)
44. J.P. Hansen, I. McDonald, *Theory of simple liquids, Third edition* (Academic Press, 2006)
45. C. Caccamo, Phys. Rep. **274**, 1 (1996)
46. J.A. Anta, A.A. Louis, Phys. Rev. B **61**, 11400 (2000)
47. O. Peyrusse, J. Phys: condensed matter **20**, 195211 (2008)
48. C.E. Starrett, D. Saumon, Phys. Rev. E **85**, 026403 (2012)
49. J. Chihara, J. Phys. C: Solid State Phys. **18**, 3103 (1985)
50. Y. Rosenfeld, N.W. Ashcroft, Phys. Rev. A **20**, 1209 (1979)
51. A. Malijevský, S. Labík, Mol. Phys. **60**, 663 (1987)
52. H. Iyetomi, S. Ogata, S. Ichimaru, Phys. Rev. A **46**, 1051 (1992)
53. W. Daughton, M. Murillo, L. Thode, Phys. Rev. E **61**, 2129 (2000)
54. Y. Rosenfeld, J. Stat. Phys. **42**, 437 (1986)
55. J.M. Ziman, Proc. Phys. Soc. **91**, 701 (1967)
56. L. Dagens, J. Phys. C **5**, 2333 (1972)
57. N.W. Ashcroft, D. Stroud, Sol. State Phys. **33**, 1 (1978)
58. S. Ichimaru, Rev. Mod. Phys. **54**, 1017 (1982)
59. G. Chabrier, J. Phys. France **51**, 1607 (1990)
60. D. Saumon, C.E. Starrett, J.D. Kress, J. Clerouin, High energy density physics **8**, 150 (2012)
61. J.D. Kress, L.A. Collins, Private communication (2012)
62. V. Recoules, F. Lambert, A. Decoster, B. Canaud, J. Clérouin, Phys. Rev. Lett. **102**, 075002 (2009)